Molecularly Engineering Polymeric Membranes for H_2/CO_2 Separation at 100 ℃ – 300 ℃

Leiqing Hu, Sankhajit Pal, Hien Nguyen, Vinh Bui, Haiqing Lin

Department of Chemical and Biological Engineering, University at Buffalo, The State University of New York, Buffalo, NY 14260, USA

Correspondence to: Haiqing Lin (Email: *haiqingl@buffalo.edu*)

ABSTRACT

Over the last two decades, polymers with superior H_2/CO_2 separation properties at 100 ℃ – 300 ℃ have gathered significant interest for H_2 purification and CO_2 capture. This timely review presents various strategies adopted to molecularly engineer polymers for this application. We first elucidate the Robeson's upper bound at elevated temperatures for H_2/CO_2 separation and the advantages of high-temperature operation (such as improved solubility selectivity and absence of CO_2 plasticization), compared with conventional membrane gas separations at ~35 ℃. Second, we describe commercially relevant membranes for the separation and highlight materials with free volumes tuned to discriminate H_2 and CO_2, including functional polymers (such as polybenzimidazole) and engineered polymers by cross-linking, blending, thermal treatment, thermal rearrangement, and carbonization. Thirdly, we succinctly discuss mixed matrix materials containing size-sieving or H_2-sorptive nano-fillers with attractive H_2/CO_2 separation properties.

KEYWORDS: Polymeric membranes; H_2/CO_2 separation; high temperatures; carbon capture

AUTHOR BIOGRAPHIES

Dr. Leiqing Hu received his B.Eng. in Thermal and Power Engineering from Shandong University in 2013 and his Ph.D. in Thermal Engineering from Zhejiang University in 2018 in China. He joined University at Buffalo (UB) as a postdoctoral associate in 2019. His research focuses on advanced membranes for gas separation and CO_2 capture.

Sankhajit Pal joined UB in 2018 to pursue a Ph.D. in Chemical Engineering. His research involves H_2/CO_2 separation by membranes. He received M. Tech. from the Indian Institute of Technology in 2015. Before joining UB, he worked as Senior Research Fellow and Assistant Professor. His previous research experience includes nanoparticle synthesis, catalysis, and reaction engineering.

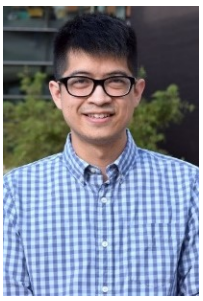

Hien Nguyen is a graduate student at UB. He earned his M.S. in Chemical Engineering from the University of California, San Diego in 2013 and B.S. in Biochemistry and Molecular Biology from the University of California, Santa Cruz in 2010. He worked as a Research Engineer at Membrane Technology and Research, Inc. from 2014 to 2016. His doctoral research focuses on the structure/property relationship of polymers for gas separation.

Vinh Bui is expected to earn a B.S. in Chemical Engineering from UB in May 2020 and plans to pursue a Ph.D. in Chemical Engineering at UB. He is working on mixed matrix materials containing MOFs for H_2/CO_2 separation.

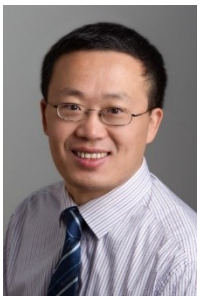

Dr. Haiqing Lin received his Ph.D. in Chemical Engineering from the University of Texas at Austin in 2005 and then joined Membrane Technology and Research, Inc. as a Senior Research Scientist. He joined UB as an assistant professor in 2013 and was promoted to associate professor in 2018. His research focuses on advanced membranes for gas separation and water purification.

INTRODUCTION

Pre-combustion CO_2 capture is one of the critical approaches to mitigate CO_2 emissions to the atmosphere.[1, 2] In this process, fossil fuels or biomass is gasified to produce syngas comprising mainly H_2 and CO. The CO is then converted to CO_2 via the water-gas shift reaction, producing ~55% H_2 and ~40% CO_2 at 200 ℃ - 300 ℃ and 20-40 bar. The shifted syngas can be separated to produce pure H_2 for turbines or ammonia plants and pure CO_2 for utilization or sequestration. Current technology for H_2/CO_2 separation is Selexol processes with physical solvents that absorb CO_2. However, these processes are energy-intensive, complex, and cumbersome. Polymeric membranes have attracted significant interest for this separation because of their high energy-efficiency, simplicity, and small footprint.[3-5] While CO_2-selective membranes often operate at temperatures below 40 °C,[6-9] H_2-selective membranes operating at the syngas temperatures (100 – 300 ℃) are desirable because they avoid the cooling of the syngas.[2] One of the membrane process designs with N_2 sweep on the permeate suggest that membranes with H_2 permeance of 300 GPU [1 GPU = 10^{-6} cm^3 (STP)/(cm^2 s cmHg)] or above and H_2/CO_2 selectivity of 30 or above provide high efficiency for membrane systems.[2]

Challenge of Polymers for H_2/CO_2 Separation

Gas transport in nonporous polymers can be described using the solution-diffusion mechanism, and gas permeability (P_A) is expressed as:[10]

$$P_A = S_A \times D_A \quad (1)$$

where S_A and D_A are gas solubility coefficient and diffusivity coefficient in the polymers, respectively. Permeability selectivity, $\alpha_{A/B}$, is the permeability ratio of the gas A to B, a combination of solubility selectivity (S_A/S_B) and diffusivity selectivity (D_A/D_B).

Table 1 shows the relevant physical properties of H_2 and CO_2. H_2 has a smaller kinetic diameter (d_A) than CO_2 and thus higher diffusivity. On the other hand, H_2 has a lower Lennard-Jones temperature (ε/k) and thus lower solubility than CO_2. The

TABLE 1 Relevant Physical Properties of H_2 and CO_2 and Parameters for H_2/CO_2 Separation. The λ_{H_2/CO_2} is derived from Robeson's empirical upper bound, and β_{H_2/CO_2} is estimated at 35 °C.[11]

Gases	d_A (Å)	ε/k (K)	ΔH_S (kJ/mol)	λ_{H_2/CO_2}	β_{H_2/CO_2} (Barrer$^{0.429}$)	$\beta_{0,H_2/CO_2}$ (Barrer$^{0.429}$)	γ_{H_2/CO_2}
H_2	2.89	60	-0.83	0.429	40	229	-543
CO_2	3.30	195	-12				

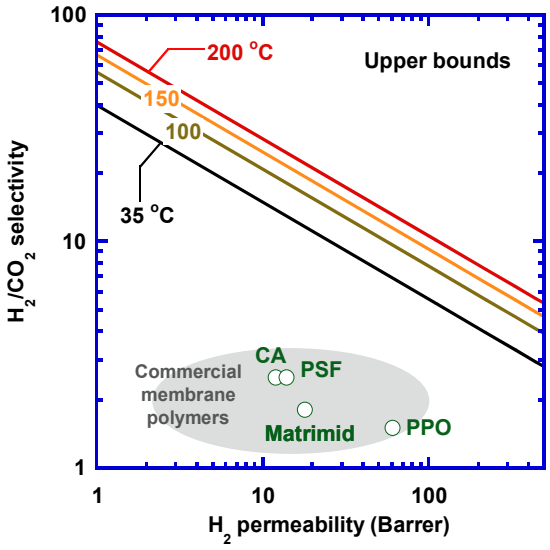

FIGURE 1 Upper bounds of H_2/CO_2 separation at 35 °C, 100 °C, 150 °C, and 200 °C calculated using the parameters shown in Table 1.[11-13] The separation properties of commercial membrane polymers were determined at 35 °C. 1 Barrer = 10^{-10} cm^3 (STP) cm/(cm^2 s cmHg).

favorable H_2/CO_2 diffusivity selectivity is offset by the unfavorable solubility selectivity, so most polymers exhibit low or moderate H_2/CO_2 selectivity (cf. Figure 1), including commercial membrane polymers, e.g., cellulose acetates (CAs),[14] polysulfone (PSf),[15] Matrimid®,[16, 17] and poly(2,6-dimethyl-1,4-phenylene oxide) (PPO).[18]

To achieve high H_2/CO_2 selectivity, polymers should have strong size-sieving ability derived from rigid chains and low free volumes, which usually lead to low H_2 permeability. Such conundrum has been articulated by the Robeson's upper bound plot (cf. Fig. 1), which is described using Equation 2: [10, 11, 19]

$$\alpha_{A/B} = \beta_{A/B} / P_A^{\lambda_{A/B}} \quad (2)$$

where $\lambda_{A/B}$ and $\beta_{A/B}$ are constants determined by the physical properties of the gases and polymers (cf. Table 1). Based on the activated diffusion model, both parameters can be expressed as:[10]

$$\lambda_{A/B} = \left(d_B/d_A\right)^2 - 1 \quad (3)$$

and

$$\beta_{A/B} = \frac{S_A}{S_B} S_A^{\lambda_{A/B}} \exp\left\{-\lambda_{A/B}\left[b - f\left(\frac{1-a}{RT}\right)\right]\right\} \quad (4)$$

where R is the gas constant, and T is the absolute temperature. The constants of a and b have values of 0.64 and 11.54 for glassy polymers, respectively. The parameter f is a measure of polymer chain rigidity and has a value of 59.2 kJ/mol for the 2008 Robeson's upper bound plots.[20] The activated diffusion model does not consider non-reversible thermal changes in polymeric materials.

Effect of Temperature on H_2/CO_2 Solubility Selectivity

The effect of temperature on gas solubility in liquids or polymers are often described using a

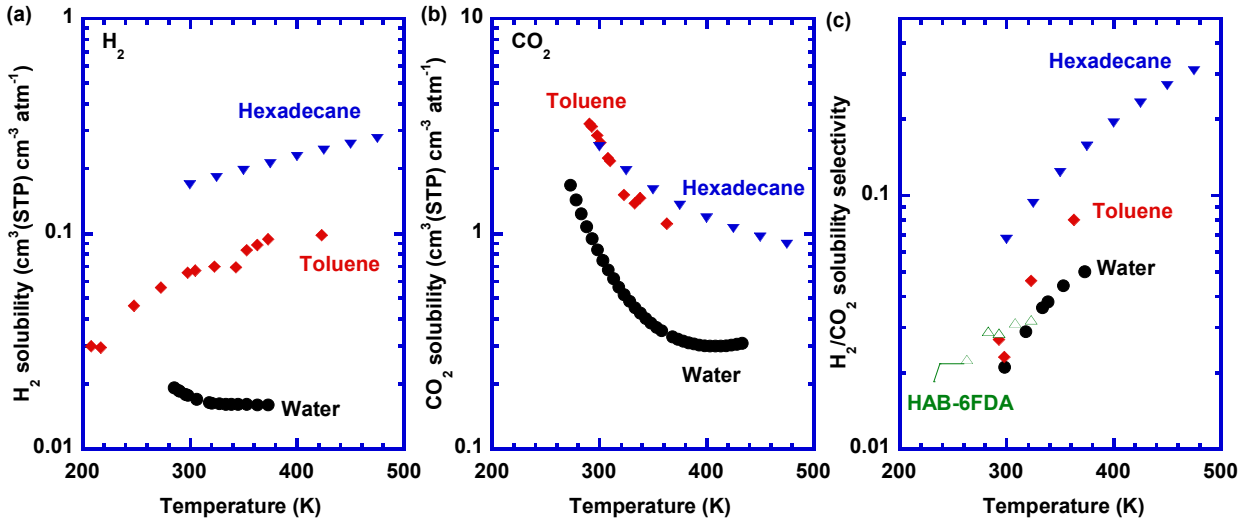

FIGURE 2 Effect of temperatures on (a) H_2 solubility, (b) CO_2 solubility, and (c) H_2/CO_2 solubility selectivity in representative liquids (e.g., water,[21, 22] hexadecane,[23-25] and toluene[26-33]) and a polyimide (HAB-6FDA).[34]

van't Hoff equation:[20]

$$S_A = S_{Ao} exp\left(-\frac{\Delta H_{SA}}{RT}\right) \quad (5)$$

where S_{Ao} is a front factor (cm^3 (STP) cm^{-3} $cmHg^{-1}$), and ΔH_{SA} is the enthalpy of sorption (kJ/mol). The ΔH_S can be correlated with ε/k using the following equation:[20]

$$\Delta H_S = R\left(500 - 10\frac{\varepsilon}{k}\right) \quad (6)$$

As H_2 has lower ε/k and higher ΔH_S than CO_2 (cf. Table 1), H_2/CO_2 solubility selectivity usually increases with increasing temperature, though it is always less than 1.

Due to the low H_2 sorption in polymers, there are very few data of H_2 solubility in polymers at elevated temperatures. Therefore, liquids are often used as surrogates for polymers because gas sorption is mainly governed by its condensability. Figure 2 displays H_2 and CO_2 solubility in representative liquids, including water, hexadecane, and toluene at various temperatures. Interestingly, increasing temperature increases H_2 solubility and decreases CO_2 solubility, both contributing to an increase in the H_2/CO_2 solubility selectivity at elevated temperatures.

Similar to the liquids, rubbery polymers such as polydimethylsiloxane (PDMS) show increased H_2 solubility with increasing temperatures.[35] On the other hand, many glassy polymers (such as polyimides and PSf) show decreased H_2 solubility with increasing temperature.[34, 35] Nevertheless, Figure 2c exhibits that H_2/CO_2 solubility selectivity in HAB-6FDA slightly increases with increasing temperature.[34] These results suggest a benefit of operating the separation at elevated temperatures. Additionally, with much lower sorption at high temperatures, the CO_2 cannot plasticize polymers, and thus, the H_2/CO_2 separation is not subject to CO_2 plasticization, which, otherwise, would weaken the size-sieving ability of polymers and then decrease the selectivity.[36]

Effect of Temperatures on H_2/CO_2 Separation Upper Bound

The effect of elevated temperatures on the upper

bound has also been rationalized using the activated diffusion model:[20]

$$\alpha_{A/B} = \beta_{0,A/B} e^{\gamma/T} / P_A^{\lambda_{A/B}} \quad (7)$$

where $\beta_{0,A/B}$ is a front factor. The γ indicates the effect of the temperature on the position of the upper bound and is expressed as:

$$\gamma = -\frac{\Delta H_{SA}}{R}\left(\lambda_{A/B} + 1\right) + \frac{\Delta H_{SB}}{R} + \lambda_{A/B} f\left(\frac{1-a}{R}\right) \quad (8)$$

Figure 1 displays the calculated upper bounds at various temperatures with the $\beta_{0,A/B}$ and γ values recorded in Table 1.[11, 12] Increasing the temperature has no effect on the slope of the upper bounds and moves up the upper bound because of the increased H_2/CO_2 solubility selectivity.

Outline of This Review

This report presents the first effort to exhaustively and critically review polymeric membranes engineered for high-temperature H_2/CO_2 separation. By contrast, polymer architectures pursued for conventional membrane applications (such as O_2/N_2 and CO_2/CH_4 separation) usually operate at 20 ℃ – 50 ℃, and therefore, design approaches can be vastly different. Polymers for H_2/CO_2 separation should be thermally stable and comprise free volume gates between their molecular sizes (2.89 Å - 3.3 Å). We first review the Robson's upper bound and commercial membranes for this application and then summarize advanced functional polymers designed for H_2/CO_2 separation. Second, various strategies to molecularly engineer polymers to improve the separation properties are described, including cross-linking, blending, and thermal treatment (such as annealing, rearrangement, and carbonization). Third, mixed matrix materials (MMMs) comprising inorganic fillers are discussed. Finally, the future development needed to bring the technology to practical use is assessed.

HIGH-PERFORMANCE POLYMERS FOR H_2/CO_2 SEPARATION

Commercially Relevant Membranes

Figure 3 presents the H_2/CO_2 separation performance of commercial membranes, Proteus™ manufactured by Membrane Technology and Research, Inc. (MTR).[2, 37] The Proteus membranes exhibited H_2 permeance of ~300 GPU with H_2/CO_2 selectivity of ~32 when tested with a coal-derived syngas containing 300 – 800 ppmv H_2S at 150 psig and 200 ℃.

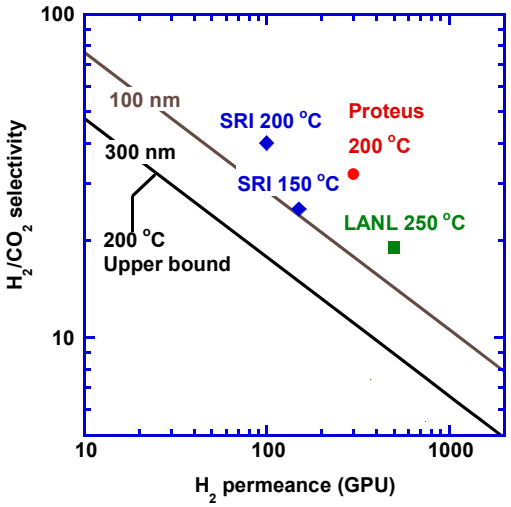

Figure 3 Commercially relevant membranes including flat sheet Proteus[37] and PBI-based HFMs from LANL[38] and SRI.[39] The upper bounds were estimated assuming 100 nm and 300 nm-thick selective layers.

Hollow fiber membranes (HFMs) based on *m*-polybenzimidazole (PBI) have been developed because of its good H_2/CO_2 separation properties (cf. Table 2) and excellent thermal stability.[40] For

example, Los Alamos National Laboratory (LANL) developed HFMs with H_2 permeance ranging from 200 to 400 GPU with H_2/CO_2 selectivity of ~ 20 at 250 ℃;[38] SRI International (SRI) reported H_2 permeance of 100 – 200 GPU and H_2/CO_2 selectivity of 40 – 20 at 150 – 250 ℃ depending on the thickness of the selective layers.[39] Due to the unknown thicknesses in these commercial membranes, a direct comparison of the selective layer materials with the upper bound is not possible. Nevertheless, Figure 3 indicates that these membranes could outperform most polymers, should they be fabricated into membranes with selective layer thicknesses of 100 nm or 300 nm.

Table 2 Structures and H_2/CO_2 Separation Properties in Dense Films of Representative Functionalized PBIs.

PBIs	Structures	Thickness (μm)	35 ℃			≈ 200 ℃	
			FFV	P_{H_2} (Barrer)	H_2/CO_2 selectivity	P_{H_2} (Barrer)	H_2/CO_2 selectivity
m-PBI[41]	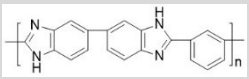	NA[a]	0.105	2.4	24	22[b]	23[b]
BTBP-PBI[40]	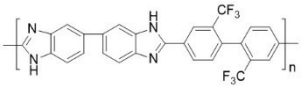	5-20	0.098	123	2.4	710[c]	7.1[c]
TADPS-IPA[41, 42]	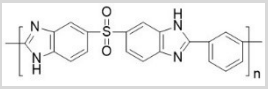	21.5	0.111	3.2	19	30[b]	25[b]
TADPS-TPA[41, 42]	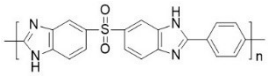	19.5	0.121	3.7	13	31[b]	18[b]
TADPS-OBA[41, 42]	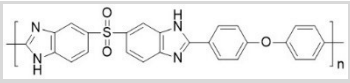	19.4	0.125	5.4	6.2	38[b]	9.7[b]
Phenylindane-PBI[40]	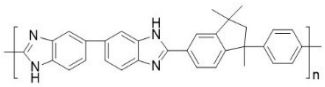	5-20	0.142	91[a]	2.0[a]	481[c]	6.5[c]
6F-PBI[40]	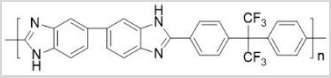	5-20	0.145	261	1.4	997[c]	5.2[c]
PFCB-PBI[40]	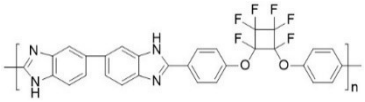	5-20	0.175	39[a]	2.4[a]	323[c]	6.6[c]

[a] Not available; [b]190 ℃; [c] 250 ℃.

Emerging Polymer Architectures

PBIs have been leading materials for H_2/CO_2 separation (with performance very close to the upper bound[11]) because of the strong size-sieving ability, which derives from π-π stacking and hydrogen bonds. Depending on the grade of the polymer and processing conditions, *m*-PBI exhibits different H_2/CO_2 separation properties, as the processing conditions are intimately related to the

membrane structures. For instance, our group reported H_2 permeability of 2.0 Barrer and H_2/CO_2 selectivity of 12 at 35 °C;[11-13] Freeman's group reported H_2 permeability of 2.4 Barrer and H_2/CO_2 selectivity of 24;[41] and a LANL group reported H_2 permeability of 3.4 Barrer and H_2/CO_2 selectivity of 16.[40]

Table 2 records a variety of functionalized PBIs, along with their structures and separation properties at 35 °C. The *m*-PBI is typically synthesized from isophthalic acid (IPA) and 3,3'-diaminobenzidine (DAB).[40-42] By replacing IPA with other diacids such as 5-tert-butyl isophthalic acid, 2,2-bis(4-carboxyphenyl)-hexafluoropropane, and terephthalic acid, PBIs with different backbone structures can be obtained, leading to higher H_2 permeability but often lower H_2/CO_2 selectivity.[40, 43, 44] Additionally, *m*-PBI is not soluble in common organic solvents and cannot be easily fabricated into asymmetric membranes by conventional solution-casting methods. Therefore, a sulfonyl-containing tetra-amine monomer, 3,3',4,4'-tetraaminodiphenylsulfone (TADPS), was used to synthesize PBIs with flexible linkages that can be soluble in common solvents.[42]

Table 2 also shows the effect of the temperature on the H_2/CO_2 separation properties. Increasing temperatures increased both H_2 permeability (because of the enhanced diffusivity) and H_2/CO_2 selectivity because of the increased solubility selectivity. By contrast, typical gas separations are often subject to decreased selectivity with increasing temperatures.[20]

Assuming that the PBIs have similar gas solubility, P_A can be correlated with polymer fractional free volume (*FFV*) using Equation 9:[12]

$$P_A = A_A \exp\left(-B_A / FFV\right) \quad (9)$$

where A_A (Barrer) is a pre-exponential factor, and B_A is a constant that increases with increasing penetrant size. The *FFV* can be estimated using the following equation:

$$FFV = \frac{V - V_0}{V} \quad (10)$$

where V is the specific volume, and V_0 is the occupied volume estimated from the van der Waal volume.

Figure 4 presents the correlation between the FFV and gas permeation properties at 35 °C. The fittings are satisfactory with a B_A value of 0.75 for H_2 and 1.4 for CO_2, consistent with their size difference. On the other hand, BTBP-PBI, phenylindane-PBI, and 6F-PBI showed much higher gas permeability than expected based on their *FFV* values, presumably because their functional groups effectively disrupt the chain packing efficiency, leading to free volume size and distribution facilitating the gas diffusion.[40]

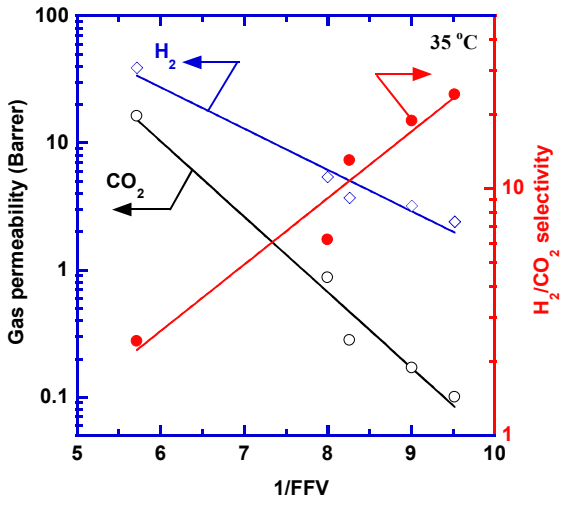

FIGURE 4 Effect of FFV on gas permeability and H_2/CO_2 selectivity at 35 °C in representative PBIs.[41, 43] The lines are the best fits of the free volume model (i.e. Equation 9).

Table 3 presents a few polymers with promising H_2/CO_2 separation properties at ~35 °C, including

syndiotactic poly(methyl methacrylate) (s-PMMA),[45] polyaniline (PANi),[46] and liquid crystalline copolyesters (LCPs) based on *p*-hydroxybenzoic acid (HBA) and 2,6 hydroxynaphthoic acid (HNA).[47] The s-PMMA exhibits unexpectedly high H_2/CO_2 selectivity.[45, 48] However, it becomes rubbery above its T_g (118 ℃) and would likely lose the size-sieving ability.

Similar to PBI, PANi has π-π stacking and H-bonds, leading to low FFV and thus low H_2 permeability and high H_2/CO_2 selectivity, though it had not been evaluated for high-temperature application. Noticeably both PBI and PANi have amine groups, indicating that the presence of the amine groups in polymers may not improve CO_2 solubility and permeability under dry conditions.[49]

LCPs have strong π-π stacking and efficient chain packing, leading to low FFV and high H_2/CO_2 selectivity.[47] Introduction of the HNA with the nonlinear naphthyl unit disrupts crystallization and hinders the rotation around the chain axis, slightly increasing T_g. $HBA_{0.8}/HNA_{0.2}$ exhibited FFV and H_2/CO_2 selectivity similar to PBI, but much lower H_2 permeability due to the chain orientation and possible crystallinity. Interestingly, increasing the HNA content (or decreasing the *m* value, cf. Table 3) had a negligible effect on the *FFV*, but dramatically increased the H_2/CO_2 selectivity. Nevertheless, these LCPs exhibited the H_2 permeability too low to be useful for practical separation and would likely lose the selectivity at ~110 ℃ or above.

TABLE 3 Structures and H_2/CO_2 Separation Properties for PMMA and LCCP at 35 ℃ and PANi at 21 ℃.

Polymers		Structure	*FFV*	T_g (℃)	H_2 permeability (Barrer)	H_2/CO_2 selectivity
PMMA[45]		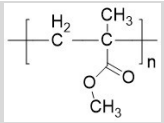	0.13	118	4.7	11
PANi[46]		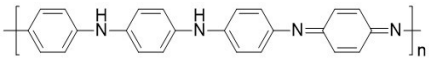	0.029	--	~1.8	23.1
LCPs[47] (HBA/ HNA)	m=0.3	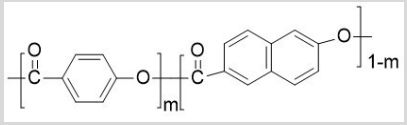	0.106	112	0.054	101
	m=0.58		0.107	109	0.063	61
	m=0.75		0.107	103	0.066	51
	m=0.8		0.107	104	0.059	27

ENGINEERING POLYMERS TO ENHANCE H_2/CO_2 SEPARATION PROPERTIES

Cross-linked Polymers

Polymers can be cross-linked to increase chain rigidity and decrease FFV, thereby enhancing size-sieving ability.[50] For example, thin-film composite membranes of highly cross-linked polyamides prepared by interfacial polymerization of *m*-phenylenediamine (MPD) and trimesoyl chloride (TMC) exhibited mixed-gas H_2 permeance of 350 GPU and H_2/CO_2 selectivity of ~50 at 140 ℃, surpassing the Robeson's upper bound.[51] Interfacial polymerization was also used to prepare highly cross-linked benzimidazole-linked polymers (BILPs), a porous organic framework. The membrane with ~400 nm thick BILP-101x exhibited a H_2/CO_2 selectivity of 40 and a H_2

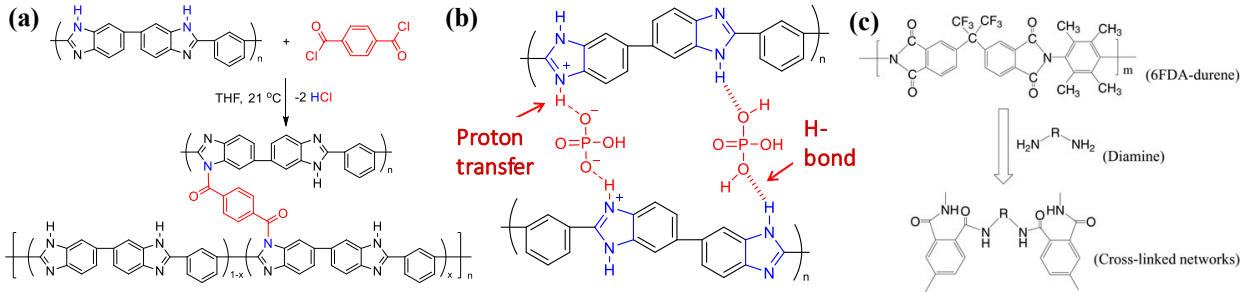

SCHEME 1 Schematic illustrations of *m*-PBI cross-linked with (a) terephthaloyl chloride and (b) phosphoric acid, and (c) 6FDA-durene cross-linked with diamines.[11, 12, 52] Reproduced with permission, Royal Society of Chemistry Publications, 2017 and 2018; and Wiley Publication, 2006.

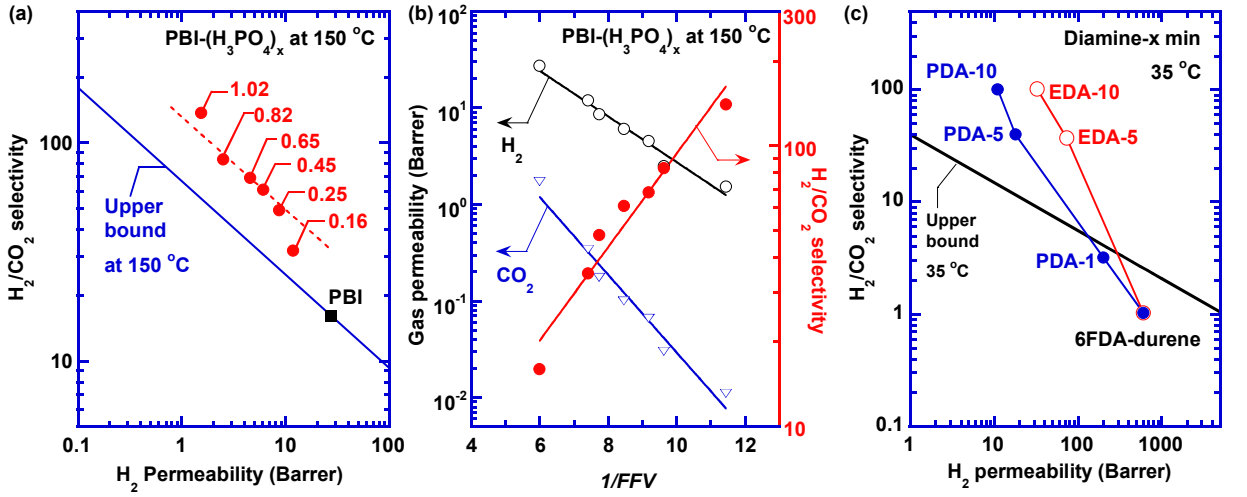

FIGURE 5 (a) H_2/CO_2 separation performance of PBIs cross-linked by H_3PO_4 with different doping levels (*x* = 0 – 1.0) at 150 ℃. (b) Modeling gas permeability and selectivity with the free volume model. Figures 5a and 5b are adapted from [12]. (c) Effect of post-cross-linking of PI (6FDA-durene) using EDA and PDA on H_2/CO_2 separation performance at 35 ℃. Data adapted from [52, 53].

permeance of 24 GPU at 150 °C.[54, 55]

Similarly, polyethylenimine (PEI) was cross-linked by poly(acrylic acid) (PAA) using a layer-by-layer approach and showed H_2/CO_2 selectivity as high as ~300 with H_2 permeability of ~4 Barrer at 23 ℃.[56] However, these PEI-based materials may not be stable above 150 ℃.

With the amine groups, PBI was cross-linked by a,a'-dibromo-p-xylene and 3,4-dichloro-tetrahydro-thiophene-1,1-dioxide in solutions before solution-casting to form solid films.[57, 58] However, H_2 permeability increased, and H_2/CO_2 selectivity decreased because the cross-linkers disrupted the packing of PBI chains during the drying processes and increased *FFV*. On the other hand, the PBI films can be post-cross-linked using terephthaloyl chloride (cf. Scheme 1a),[11] polyprotic acids (such as phosphoric acid, cf. Scheme 1b),[12] and 1,3,5-Tris(bromomethyl) benzene (TBB),[59] decreasing *FFV*.

Figure 5a demonstrates the superior H_2/CO_2 separation properties at 150 ℃ in the PBI cross-linked by H_3PO_4 at different doping levels (*x*, defined as the molar ratio of H_3PO_4 to the PBI repeating units).[12] Increasing *x* decreased H_2 permeability and increased H_2/CO_2 selectivity. At *x* = 1.0, the H_2/CO_2 selectivity reached as high as 140, which is the highest among the polymers reported. Such changes can be explained using the free volume model. As shown in Figure 5b, increasing the *x* values decreased the *FFV* and thus gas permeability but increased the selectivity. The PBI-$(H_3PO_4)_{0.16}$ was further tested with H_2/CO_2 mixtures in the presence of water vapor 150 ℃ and demonstrated long-term stability.

As a flexible material platform, polyimides (PIs) exhibit a strong size-sieving ability for the separation of O_2 (3.46 Å) and N_2 (3.64 Å), and CO_2 and CH_4 (3.8 Å), but not for H_2/CO_2 separation. On the other hand, polyimides were cross-linked by diamines to improve the H_2/CO_2 selectivity (cf. Scheme 1c).[53, 60-69] For example, the exposure of 6FDA-durene films to vapor-phase ethylenediamine (EDA) or 1,3-diaminopropane (PDA) for 10 min increased H_2/CO_2 selectivity from 1.0 to ~100 at 35 ℃, as shown in Figure 5c.[52, 53] However, the cross-linked Matrimid, 6FDA-durene, and 6FDA-ODA were not stable above 100 ℃ because the reaction of imide rings and diamines reverses.[60-62, 70, 71] Interestingly, when P84™ (a polyimide) was cross-linked with 1,4-butylene diamine (BuDA), the samples were stable up to 150 ℃ and showed H_2 permeability of 47 Barrer and H_2/CO_2 selectivity of 14 at 100 ℃, which is on the Robeson's upper bound.[72]

The cross-linking of the polyimides was often performed with thick films (50 μm), and the reaction only occurred on the surface and not evenly in bulk (as indicated by the low gel content in the cross-linked samples).[52, 62, 66, 68] Therefore, the structure/property relationship is yet to be elucidated in these cross-linked polyimides.

Polymer Blends

PBI has been blended with polymers with higher H_2 permeability and lower H_2/CO_2 selectivity than PBI, aiming to increase permeability while retaining the selectivity.[73, 74] These blends are often phase-separated, and the gas permeability (P_b) can be described using the Maxwell model:[74]

$$P_b = P_c\left[\frac{P_d + 2P_c - 2\phi_d\left(P_c - P_d\right)}{P_d + 2P_c + \phi_d\left(P_c - P_d\right)}\right] \quad (11)$$

where ϕ_d is the volume fraction of the dispersed phase, and P_d and P_c are gas permeability of the dispersed phase and continuous phase, respectively. The model predicts that blending highly permeable polymers in the continuous PBI phase can increase H_2 permeability and retain the H_2/CO_2 selectivity from the PBI.

Figure 6 illustrates the benefits of dispersing a highly permeable polyimide, 6FDA-DAM:DABA (3:2) (6FDD), in the PBI.[73] 6FDD showed H_2 permeability of 100 Barrer and H_2/CO_2 selectivity of only 1.9 at 35 ℃. An immiscible blend of 6FDD:PBI (50:50) exhibited H_2 permeability of 7.5 Barrer (much higher than 1.1 Barrer for PBI) and H_2/CO_2 selectivity of 10 (comparable to 11 for PBI). The blend showed H_2 permeability higher than predicted by the Maxwell model (4.1 Barrer) because of the extra free volume derived from the uncontrollable phase separation. When 2-methylimidazole (2-MI) was added in the casting solution (9 wt%) to improve interface stability, H_2/CO_2 selectivity increased to 40, and H_2

permeability decreased to 4.0 Barrer because of the residual 2-MI at the interface after thermal annealing.[73] Similarly, PBI was blended with HAB-6FDA-CI (with H_2 permeability of 24 Barrer and H_2/CO_2 selectivity of 4.3 at 35 ℃).[74] 1-Methylimidazole (1-MI) was added in the casting solution as a compatibilizer and then removed during the thermal annealing. Introducing 33 wt% HAB-6FDA-CI in PBI increased H_2 permeability from 3.7 Barrer to 4.3 Barrer while retaining the H_2/CO_2 selectivity (~16).

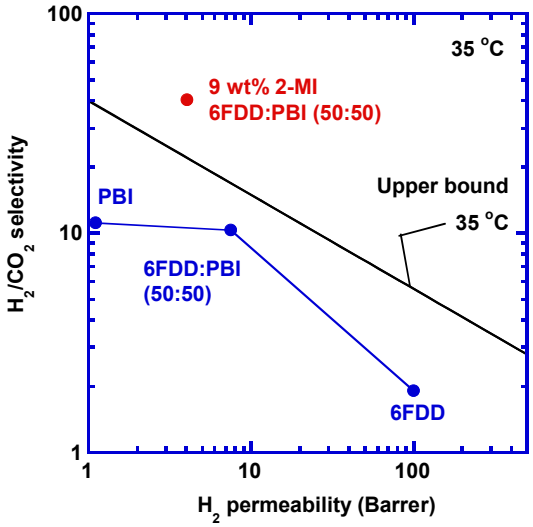

FIGURE 6 Effect of blending 6FDD with PBI and a compatibilizer (2-MI) on the H_2/CO_2 separation properties at 35 ℃.[73]

PBI was also blended with glassy polymers other than PIs. For example, thermosets of PBI and poly(melamine co-formaldehyde) (PMF) were synthesized and showed H_2 permeability of 57 Barrer and H_2/CO_2 selectivity of 13 at 250 ℃.[75] Asymmetric membranes based on blends of PBI and polymers of intrinsic microporosity (PIM) displayed H_2 permeance of 58 GPU and H_2/CO_2 selectivity of 24 at 250 ℃.[76]

PBI can be blended with sulfonated polyphenylsulfone (sPPSU) and cross-linked with α,α´-dibromo-p-xylene, leading to H_2 permeability of 46 Barrer and H_2/CO_2 selectivity of 9.9 at 150 °C.[77] The blends were fabricated into HFMs with H_2 permeance of 17 GPU and H_2/CO_2 selectivity of 9.7 at 90 ℃.[78, 79] When a blend of PBI/Matrimid (75/25) was cross-linked with *p*-xylene diamine, the H_2/CO_2 selectivity increased from 9.4 to 26, and H_2 permeability decreased from 5.5 Barrer to 3.6 Barrer.[80]

Thermally Treated, Rearranged, and Carbonized Polymers

Thermal treatment is a powerful route to modify polymer morphology. PBI can be grafted with thermally labile groups, such as low molecular weight poly(ethylene oxide) (PEO) and poly(propylene carbonate) (PPC), which can then be removed and created "nanovoids."[81] For instance, thermal annealing of PBI grafted with 13 wt% PEO at 400 ℃ increased H_2 permeability from 4.0 Barrer to 6.9 Barrer and H_2/CO_2 selectivity from 7.5 to 10 at 35 ℃. Similarly, thermal treatment of a PBI/PANi (80/20) blend increased H_2 permeability from 0.98 Barrer to 5.6 Barrer and H_2/CO_2 selectivity from 5.7 to 15 at 30 ℃.[82]

Polyimides with orthohydroxy groups can be thermally rearranged, yielding TR polymers with rigid structures and strong size-sieving ability and cavities, leading to high gas permeability.[83] However, similar to polyimides, TR polymers often have cavities too large to discriminate H_2 and CO_2 separation. On the other hand, poly(benzoxazole-co-amide) (PBOA) was prepared from poly(o-hydroxyamide-co-amide) through in-situ thermal cyclization reaction, leading to small cavities.[84] An example TR polymer (PHBOA(8:2)) exhibits H_2 permeability of 1.8 Barrer and H_2/CO_2 selectivity of 8.4 at 35 ℃, which varied to 26.8 Barrer and 8.0 at 210 ℃, respectively. PBI was also blended with a

precursor HAB-6FDA-CI with a compatibilizer of 1-MI before the thermal rearrangement at 400 ℃.[74] The rearrangement of 20/80 HAB-6FDA-CI/PBI had minimal effect on H_2 permeability but unexpectedly increased the H_2/CO_2 selectivity from 17 to 42 at 35 ℃ because of the ordering and densification of the PBI phase facilitated by the 1-MI during the thermal treatment.

Polymers can be carbonized to form carbon molecular sieves (CMS) with strong size-sieving abilities. Figure 7a illustrates the carbonization of PBI. The resulting morphology features a bimodal pore size distribution populated with micropores (7–20 Å) providing high gas permeability and ultramicropores (< 7 Å) yielding the strong size-sieving ability.[4, 85-87] Fig. 7b presents the effect of the carbonization temperature for PBI on pure-gas H_2 and CO_2 permeability at 100°C and 7.4 atm. When carbonized at 700 ℃, the obtained PBI@700 exhibits H_2 permeability almost 2 orders of magnitude higher than PBI with a decrease of H_2/CO_2 selectivity from 14 to 8.7 at 100°C. However, PBI@900 exhibits remarkably higher H_2/CO_2 selectivity of 80 with lower H_2 permeability than PBI@700, presumably because of the densification and formation of smaller pore sizes.[86]

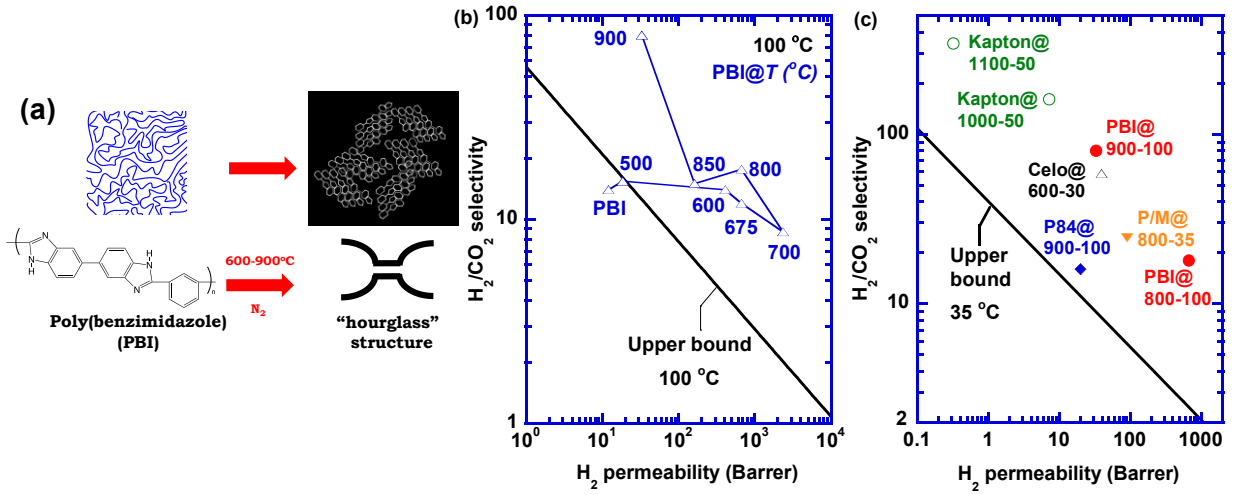

FIGURE 7 (a) Schematic of the carbonization of PBI to create microporous structures and ultra-microporous channels; (b) Pure-gas H_2/CO_2 separation performance for various PBI CMS samples. (c) Comparison of various carbonized polymers, including PBI@700-100 and PBI@900-100,[86] P/M@800-35,[88] P84@900-100,[89] Celo@600-30,[90] and Kapton@1000-50 and Kapton@1100-50.[91] The last number is the testing temperature (°C) for gas permeation. Figures (a) and (b) are reproduced with permission, ACS Publication, 2019.

Other polymers have also been pyrolyzed at high temperatures to achieve superior H_2/CO_2 separation properties, as shown in Figure 7c. For instance, Kapton with a low FFV (0.098) was carbonized at 1000 ℃ (Kapton@1000) and showed extremely high H_2/CO_2 selectivity of 161 and H_2 permeability of 7.2 Barrer at 50 ℃.[91] Kapton@1100 exhibited even higher H_2/CO_2 selectivity (343) with H_2 permeability of only 0.32 Barrer at 50 ℃. HFMs of P84 were carbonized at 900 ℃, increasing H_2/CO_2 selectivity from 6.6 to 16.4 and decreasing H_2 permeance from 48 GPU to 8.2 at 100 ℃.[89] Carbonization of cellophane at 600 ℃ (Celo@600) yields H_2 permeability of 39 Barrer

and H_2/CO_2 selectivity of 59 at 30 °C.[90]

Carbonization can be combined with blending and cross-linking to improve the separation properties. For example, carbonization of a 50/50 PBI/Matrimid blend at 800 °C (P/M@800) increased H_2 permeability from 13 Barrer to 324 Barrer and H_2/CO_2 selectivity from 6.0 to 8.8 at 35 °C.[88] On the other hand, if the blend was cross-linked via 5-day exposure to *p*-xylene diamine before the carbonization, the CMS exhibited H_2 permeability of ≈ 90 Barrer and H_2/CO_2 selectivity of ≈ 24.

MIXED MATRIX MATERIALS (MMMs)

MMMs comprising polymers and nano-fillers have attracted interests for membrane gas separations because the MMMs synergistically combine the good processability of polymers and the unique properties of the fillers.[92, 93] For example, fillers with high porosity and large pores can be used to increase permeability but cannot increase selectivity, such as COF NUS-3 with hexagonal channels of 1.8 nm[94] and zeolite MCM-22 with pore sizes of 0.6 nm and 1.4 nm.[95] Instead, this review focuses on the MMMs with improved diffusivity selectivity or solubility selectivity.

MMMs with Enhanced H_2/CO_2 Diffusivity Selectivity

Figure 8a shows the schematic of the MMMs comprising porous fillers with a strong size-sieving ability for H_2/CO_2 separation. Metal-organic frameworks (MOFs) have emerged as a promising material platform because of their well-controlled pore sizes, such as ZIFs and UiO-66-type MOFs.

Figures 8b and 8c present H_2/CO_2 separation properties of PBI-based MMMs at 35 °C and 150 - 230 °C, respectively. Incorporation of MOFs can increase both H_2 permeability and H_2/CO_2 selectivity. For example, ZIF-7 has a pore aperture of 3.1 Å between the kinetic diameter of H_2 and CO_2 (cf. Table 1). Due to the pore breathing effect, CO_2 can swell the ZIF-7 crystals, leading to an experimental H_2/CO_2 selectivity of 13 in a ZIF-7 thin layer.[96] On the other hand, adding 50 wt% ZIF-7 in PBI [PBI/ZIF-7(50)] increased H_2 permeability from 3.7 Barrer to 26 Barrer and H_2/CO_2 selectivity from 8.7 to 15 at 35 °C.[97] At 180 °C, H_2/CO_2 selectivity in PBI/ZIF-7(50) decreased to 8.5. While the effect of the ZIF-7 loading on CO_2 permeability can be described using the Maxwell model, the H_2 permeability was much higher than the predicted values.[97]

With aperture sizes of 11.6 Å and 3.4 Å, ZIF-8 has a theoretical H_2 permeability of 22,000 Barrer (calculated using diffusivity obtained from kinetic uptake measurements) and H_2/CO_2 selectivity of 6.7 at 35 °C.[98, 99] When supported on polydopamine-functionalized stainless-steel-nets, a ZIF-8 layer showed a H_2/CO_2 selectivity of 8.8 at 100 °C,[100] similar to the theoretical value. Interestingly, adding 30 wt% ZIF-8 in PBI increased H_2 permeability from 3.7 Barrer to 105 Barrer and H_2/CO_2 selectivity from 8.6 to 12 at 35 °C.[101] PBI-ZIF-8(30) was fabricated into HFMs and exhibited H_2 permeability of 470 Barrer and H_2/CO_2 selectivity as high as 26 at 230 °C.[102] PBI/ZIF-8(10) based HFMs exhibited H_2 permeability of ~33 Barrer (estimated based on permeance of 107 GPU and the selective layer thickness of 307 nm) and H_2/CO_2 selectivity of 16 at 150 °C.[103] Another PBI/ZIF-8-based HFMs showed H_2 permeance of 22 GPU and H_2/CO_2 selectivity of 22 at 250 °C, and the selective layer thickness was not reported.[104] The increased selectivity with the ZIF-8 loading cannot be explained using the Maxwell model.

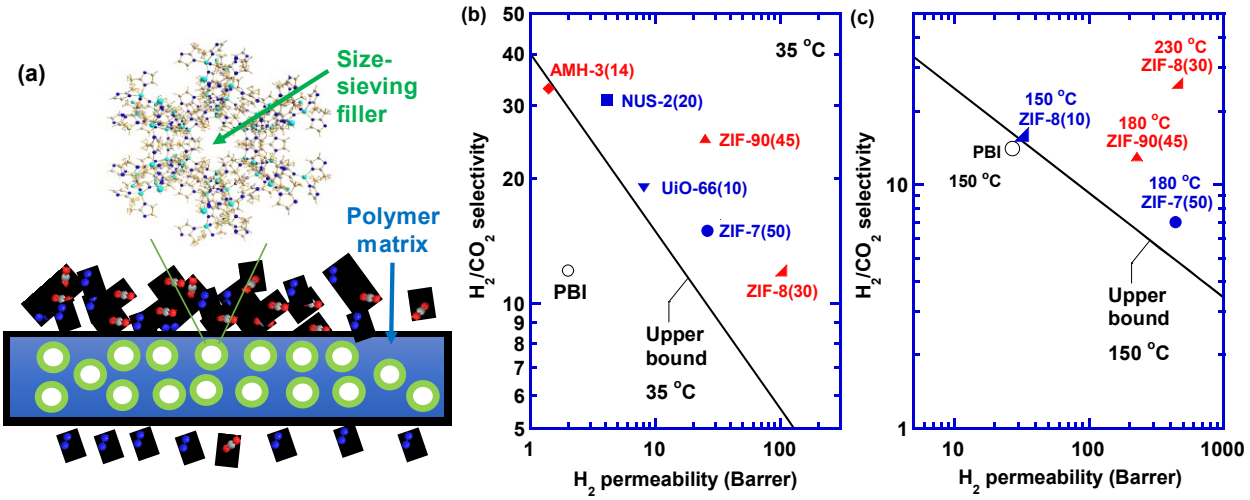

FIGURE 8 (a) Schematic of MMMs with enhanced H_2/CO_2 diffusivity selectivity. Pure-gas H_2/CO_2 separation performance for PBI-based MMMs at (b) 35 °C and (c) 150 °C - 230 °C, including PBI,[11] AMH-3(14),[95] ZIF-7(50),[97] ZIF-8(10),[103] ZIF-8(30),[101, 102] ZIF-90(45),[105] UiO-66(10),[106] and NUS-2(20).[94] The numbers in the brackets refer to the loaing of the filler (wt%).

With an aperture size of 3.5 Å and pore size of 11.2 Å, ZIF-90 showed an ideal H_2/CO_2 selectivity of 7.2, as determined for a dense layer on a porous ceramic support.[107] However, PBI/ZIF-90(45) exhibited H_2 permeability of 24 Barrer and H_2/CO_2 selectivity of 25 at 35 °C, which changed to 227 Barrer and 13 at 180 °C, respectively.[105] Additionally, UiO-66 has triangular pores of ~ 6 Å, and its thin layer exhibited a H_2/CO_2 selectivity of 5.1.[108] When UiO-66(Hf)-$(OH)_2$ with reduced pore sizes of ~ 4 Å was incorporated in PBI at 10 wt%, H_2 permeability increased from 3.6 Barrer to 8.1 Barrer, and H_2/CO_2 selectivity increased from 9.0 to 19 at 35 °C.[106]

PBI was also blended with other nano-fillers to improve the H_2/CO_2 separation properties. For instance, two-dimensional layers of COF NUS-2 with pore sizes of 0.8 nm were incorporated at 10 wt% and increased H_2/CO_2 selectivity to 31.[94] Layered silicates of AMH-3 pore size of 3.4 Å were sequentially intercalated by dodecylamine and DL-histidine before the dispersion. At 3 wt%, the nanoporous silicate increased H_2/CO_2 selectivity from 15 to 40 at 35 °C.[95]

Table 4 shows that cross-linked polyimides can also be blended with nano-fillers (mainly MOFs) to improve the H_2/CO_2 separation properties. For example, ZIF-71 has an aperture size of 4.2 Å.[109] 6FDA-durene/ZIF-71(10) was cross-linked with *tris*(2-aminoethyl) amine (TAEA) vapor for 1 h, which increased H_2/CO_2 selectivity to 50 and retained H_2 permeability at ~270 Barrer at 35 °C.[67, 110] MMMs containing 6FDA-durene and ZIF-8[111, 112] or Matrimid and ZIF-90[113] were cross-linked with EDA vapor and achieved superior separation performance at 35 °C. However, the cross-linking with diamine is reversible at high temperatures, causing a dramatic decrease of H_2/CO_2 selectivity at 150 °C for 6FDA-durene/ZIF-71(10) (cf. Table 4).

Table 4 also records two other MMMs with interesting H_2/CO_2 separation properties. Nano-sodalite (Nano-SOD) crystals have an aperture size

of 2.8 Å, and 10 wt% loading in polyetherimide led to H_2 permeability of 7155 Barrer with H_2/CO_2 selectivity of ~28 at 25 °C.[114] PMMA was blended with CAU-1-NH_2 (with an aperture size of 3–4 Å) and showed very high H_2 permeability with good selectivity.[115] Additionally, when the ZIF-8 (~0.62 wt%) was incorporated into the polyamide-based TFC membranes prepared by interfacial polymerization, H_2/CO_2 selectivity increased from 7.9 to 15, and H_2 permeance decreased from 500 GPU to 320 GPU at 180 °C.[116]

TABLE 4 Non-PBI-based MMMs with Promising Separation Performance at Different Temperatures.

MMMs			Temperature	H_2 permeability	H_2/CO_2	Ref.
Polymers	Filler(wt%)	Cross-linker	(°C)	(Barrer)	selectivity	
6FDA-durene	None	None	35	220	0.2	67
	ZIF-71(10)	TAEA	35	270	50	
			150	1600	2.4	
6FDA-durene	None	TAEA	35	300	47	110
	ZIF-71(20)	TAEA	35	581	252	
6FDA-durene	None	EDA	35	117	24	111
	ZIF-8(50)	EDA	35	501	29	
6FDA-durene	None	EDA	35	52	130	112
	ZIF-8(33.3)	EDA	35	284	12	
Matrimid 5218	None	None	25	28	3.5	113
	ZIF-90(25)	EDA	25	19	9.5	
Polyetherimide	None	None	25	14	NA	114
	Nano-SOD(10)	None	25	7,155	28	
PMMA	None	None	35	5000	3	115
	CAU-1-NH_2(15)	None	35	11,000	13	
Polyamides	None	None	180	500[a]	7.9	116
	ZIF-8(0.62)	None	180	320[a]	15	

[a]: permeance with a unit of GPU, instead of permeability.

MMMs with Enhanced H_2/CO_2 Solubility Selectivity

Palladium (Pd) can chemically dissolve H_2 to form palladium hydrides (PdH_x), providing extremely high H_2 reversible sorption up to 500−1000 cm^3 (STP) cm^{-3},[35, 117] much higher than that in polymers (~ 0.1 cm^3 (STP) cm^{-3}). Therefore, Pd nanoparticles were dispersed in the polymer matrix to improve H_2/CO_2 separation performance. For instance, the MMMs containing 2−4 wt% Pd into PBI exhibited H_2/CO_2 selectivity of 19 at 200 °C,[118] and incorporation of 23 wt% Pd in PBI-HFMs showed H_2/CO_2 selectivity of 10 at 60 °C.[119] These selectivity values are similar to that in the pure PBI, presumably because of the low Pd loading.

Figure 9a displays the dispersion of high content of Pd nanoparticles (~ 5 nm in diameter) in PBI to enhance H_2/CO_2 separation properties. For

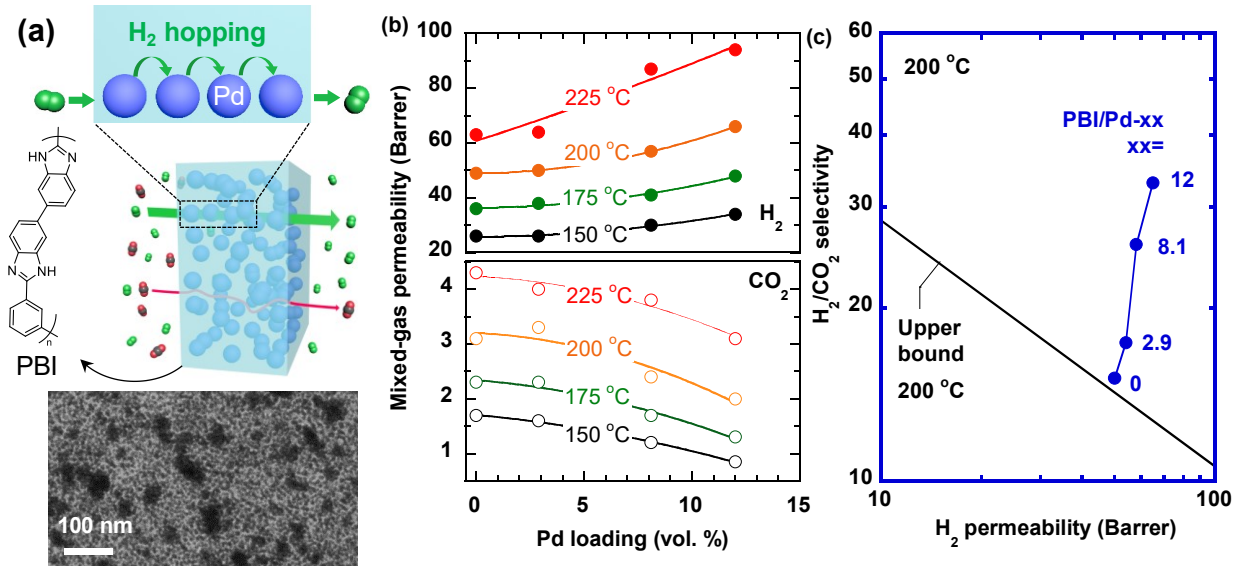

FIGURE 9 (a) Schematic of H_2 hopping among Pd nanoparticles in PBI-based MMMs with enhanced H_2 solubility.[13] (b) Effects of Pd loading on H_2 and CO_2 permeability at various temperatures. (c) Pure-gas H_2/CO_2 separation performance of Pd/PBI-xx at 200 ℃, where xx refers to the volume percentage of the Pd nanoparticles in the MMMs. Figures (a) and (b) are reproduced with permission. Wiley, 2019.

example, the MMM containing 12 vol% Pd exhibited H_2 solubility of 10 cm^3 (STP) cm^{-3} atm^{-1} and H_2/CO_2 solubility selectivity of 28 (near three orders of magnitude higher than that in PBI).

Figure 9b elucidates the effect of the Pd loading on gas permeability at various temperatures. Increasing the loading increased H_2 permeability because of the enhanced H_2 solubility. Additionally, the presence of Pd nanoparticles decreased CO_2 solubility and diffusivity. Both contributed to the increased H_2/CO_2 selectivity. The effect of the Pd loading on the gas permeability can be satisfactorily described using the Maxwell model. Figure 9c demonstrates that increasing the Pd loading increased both H_2 permeability and H_2/CO_2 selectivity, above the upper bound.[13] The MMMs were demonstrated with stable permeability and selectivity in the presence of water vapor and ~5 ppm H_2S.

CONCLUSIONS

The need for operation at elevated temperatures for H_2/CO_2 separation presents a new opportunity for the evolvement of polymeric membranes. Increasing the temperature increases H_2 permeability and H_2/CO_2 solubility selectivity and could increase H_2/CO_2 selectivity. Therefore, increasing the temperature moves up the permeability/selectivity upper bound in the Robeson's plot. This review summarizes emerging polymeric materials with superior H_2/CO_2 separation properties, and the associated design strategies, which can also guide membrane development for other gas separations.

One effective design strategy to increase the H_2/CO_2 selectivity in polymers is to decrease free volume and increase size-sieving ability, as exampled by thin-film composite membranes of Proteus and PBI-based HFMs. PBIs also serve as the base polymers for a variety of modifications, such as cross-linking, thermal treatment, and

carbonization. Cross-linking and thermal treatment often tighten the structure, increasing the selectivity but decreasing H_2 permeability. The carbonization of PBI may increase both permeability and selectivity, depending on the conditions. Polyimides are another flexible material platform, but they usually do not have good H_2/CO_2 selectivity. Polyimides can be cross-linked with diamines to dramatically increase the selectivity. However, the cross-linking is reversible at high temperatures, leading to low selectivity at 150 ℃ or above.

H_2/CO_2 selectivity can also be increased by dispersing Pd NPs in PBI to improve the solubility selectivity. Increasing the Pd loading increases both H_2 permeability and the selectivity, which can be satisfactorily described using the Maxwell model.

PBI can be blended with highly permeable polymers to form phase-separated blends with a continuous PBI phase, which increase H_2 permeability while retaining the H_2/CO_2 selectivity. MMs comprising inorganic nano-fillers have been extensively explored, including MOFs. Interestingly, most MOFs (such as ZIF-7, ZIF-8, ZIF-71, ZIF-90, etc.) do not have good H_2/CO_2 selectivity. However, after incorporation into the polymers (PBI or polyimides), the selectivity can be significantly improved, which cannot be explained using the Maxwell model.

ACKNOWLEDGMENTS

This work was funded by the U.S. Department of Energy (DOE) award No. DE-FE0031636 and the U.S. National Science Foundation (NSF) grant number 1804996.

REFERENCES AND NOTES

1. Miller, D. C.; Litynski, J. T.; Brickett, L. A.; Morreale, B. D. *AICHE J.* **2016,** 62, (1), 2-10.
2. Merkel, T. C.; Zhou, M. J.; Baker, R. W. *J. Membr. Sci.* **2012,** 389, 441-450.
3. Park, H. B.; Kamcev, J.; Robeson, L. M.; Elimelech, M.; Freeman, B. D. *Science* **2017,** 356, (6343), eaab0530.
4. Koros, W. J.; Zhang, C. *Nat. Mater.* **2017,** 16, (3), 289-297.
5. Shao, L.; Low, B. T.; Chung, T. S.; Greenberg, A. R. *J. Membr. Sci.* **2009,** 327, 18-31.
6. Li, S.; Jiang, X.; Yang, X.; Bai, Y.; Shao, L. *J. Membr. Sci.* **2019,** 570, 278-285.
7. Jiang, X.; He, S.; Li, S.; Bai, Y.; Shao, L. *J. Mater. Chem. A* **2019,** 7, (28), 16704-16711.
8. Lin, H.; He, Z.; Sun, Z.; Ng, A.; Baker, R. W.; Merkel, T. C. *J. Membr. Sci.* **2015,** 493, 794-806.
9. Lin, H.; Van Wagner, E.; Freeman, B. D.; Toy, L. G.; Gupta, R. P. *Science* **2006,** 311, (5761), 639-642.
10. Freeman, B. D. *Macromolecules* **1999,** 32, (2), 375-380.
11. Zhu, L.; Swihart, M.; Lin, H. *J. Mater. Chem. A* **2017,** 5, (37), 19914-19923.
12. Zhu, L.; Swihart, M.; Lin, H. *Energy Environ. Sci.* **2018,** 11, (1), 94-100.
13. Zhu, L.; Yin, D.; Qin, Y.; Konda, S.; Zhang, S.; Zhu, A.; Liu, S.; Xu, T.; Swihart, M. T.; Lin, H. *Adv. Funct. Mater.* **2019,** 29, (36), 1904357.
14. Puleo, A. C.; Paul, D. R.; Kelley, S. S. *J. Membr. Sci.* **1989,** 47, (3), 301-332.
15. Aitken, C. L.; Koros, W. J.; Paul, D. R. *Macromolecules* **1992,** 25, (13), 3424-3434.
16. Vu, D. Q.; Koros, W. J.; Miller, S. J. *J. Membr. Sci.* **2003,** 211, (2), 311-334.
17. Zhang, Y. F.; Musseman, I. H.; Ferraris, J. P.; Balkus, K. J. *J. Membr. Sci.* **2008,** 313, (1-2), 170-

181.
18. Koros, W.; Fleming, G.; Jordan, S.; Kim, T.; Hoehn, H. *Prog. Polym. Sci.* **1988,** 13, (4), 339-401.
19. Robeson, L. M. *J. Membr. Sci.* **2008,** 320, (1-2), 390-400.
20. Rowe, B. W.; Robeson, L. M.; Freeman, B. D.; Paul, D. R. *J. Membr. Sci.* **2010,** 360, (1-2), 58-69.
21. Morrison, T. J.; Billett, F. *J. Chem. Soc.* **1952**, (Oct), 3819-3822.
22. Carroll, J. J.; Slupsky, J. D.; Mather, A. E. *J. Phys. Chem. Ref. Data* **1991,** 20, (6), 1201-1209.
23. Cukor, P. M.; Prausnit, J. M. *J. Phys. Chem.* **1972,** 76, (4), 598-601.
24. Makranczy, J.; Megyery-Balog, K. M.; Rusz, L.; Patyi, L. *Hung. J. Ind. Chem.* **1976,** 4, (1), 269-280.
25. Tremper, K. K.; Prausnitz, J. M. *J. Chem. Eng. Data* **1976,** 21, (3), 295-299.
26. Lay, E. N.; Taghikhani, V.; Ghotbi, C. *J. Chem. Eng. Data* **2006,** 51, (6), 2197-2200.
27. Tochigi, H.; Hasegawa, K.; Asano, N.; Kojima, K. *J. Chem. Eng. Data* **1998,** 43, (6), 954-956.
28. Chang, C. J.; Chen, C. Y.; Lin, H. S. *J. Chem. Eng. Data* **1995,** 40, (4), 850-855.
29. Yin, J.; Tan, C. *Fluid Ph. Equilibria* **2006,** 242, (2), 111-117.
30. Brunner, E. *J. Chem. Eng. Data* **1985,** 30, (3), 269-273.
31. Jauregui-Haza, U. J.; Pardillo-Fontdevila, E. J.; Wilhelm, A. M.; Delmas, H. *Lat. Am. Appl. Res.* **2004,** 34, (2), 71-74.
32. Zirrahi, M.; Azinfar, B.; Hassanzadeh, H.; Abedi, J. *J. Chem. Eng. Data* **2015,** 60, (6), 1592-1599.
33. Ipatiev, V. V.; Levina, M. I. *Zhur. Fiz. Khim.* **1935,** 6, 632-9.
34. Stevens, K. A.; Smith, Z. P.; Gleason, K. L.; Galizia, M.; Paul, D. R.; Freeman, B. D. *J. Membr. Sci.* **2017,** 533, 75-83.
35. Smith, Z. P.; Tiwari, R. R.; Murphy, T. M.; Sanders, D. F.; Gleason, K. L.; Paul, D. R.; Freeman, B. D. *Polymer* **2013,** 54, (12), 3026-3037.
36. Galizia, M.; Chi, W. S.; Smith, Z. P.; Merkel, T. C.; Baker, R. W.; Freeman, B. D. *Macromolecules* **2017,** 50, (20), 7809-7843.
37. Merkel, T. C. *Novel polymer membrane process for pre-combustion CO_2 capture from coal-fired syngas, Final report to the U.S. DOE, FE0001124*; Membrane Technology and Research, Inc., Newark, CA: 2011.
38. Singh, R. P.; Dahe, G. J.; Dudeck, K. W.; Welch, C. F.; Berchtold, K. A. *Energy Procedia* **2014,** 63, 153-159.
39. Wang, S.; Li, X.; Wu, H.; Tian, Z.; Xin, Q.; He, G.; Peng, D.; Chen, S.; Yin, Y.; Jiang, Z.; Guiver, M. *Energy Environ. Sci.* **2016,** 9, (6), 1863-1890.
40. Li, X.; Singh, R. P.; Dudeck, K. W.; Berchtold, K. A.; Benicewicz, B. C. *J. Membr. Sci.* **2014,** 461, 59-68.
41. Stevens, K. A.; Moon, J. D.; Borjigin, H.; Liu, R.; Joseph, R. M.; Riffle, J. S.; Freeman, B. D. *J. Membr. Sci.* **2020,** 593, 117427.
42. Borjigin, H.; Stevens, K. A.; Liu, R.; Moon, J. D.; Shaver, A. T.; Swinnea, S.; Freeman, B. D.; Riffle, J. S.; McGrath, J. E. *Polymer* **2015,** 71, 135-142.
43. Kumbharkar, S. C.; Karadkar, P. B.; Kharul, U. K. *J. Membr. Sci.* **2006,** 286, (1-2), 161-169.
44. Singh, R. P.; Li, X.; Dudeck, K. W.; Benicewicz, B. C.; Berchtold, K. A. *Polymer* **2017,** 119, 134-141.
45. Min, K.; Paul, D. R. *J. Polym. Sci., Part B: Polym. Phys.* **1988,** 26, (5), 1021-1033.
46. Illing, G.; Hellgardt, K.; Schonert, M.; Wakeman, R. J.; Jungbauer, A. *J. Membr. Sci.* **2005,** 253, (1-2), 199-208.
47. Weinkauf, D. H.; Paul, D. R. *J. Polym. Sci., Part B: Polym. Phys.* **1992,** 30, (8), 837-849.
48. Raymond, P. C.; Paul, D. R. *J. Polym. Sci., Part B: Polym. Phys.* **1990,** 28, (11), 2079-2102.
49. Zhu, L.; Tian, D.; Shin, D.; Jia, W.; Bae, C.; Lin, H. *J. Polym. Sci., Part B: Polym. Phys.* **2018,** 56, (18),

1239-1250.
50. Zhu, L.; Omid, M.; Lin, H., Manipulating Polyimide Nanostructures via Cross linking for Membrane Gas Separation. In *Membranes for Gas Separations*, Carreon, M. A., Ed. World Scientific: 2017; Vol. 1, pp 243-270.
51. Ali, Z.; Pacheco, F.; Litwiller, E.; Wang, Y.; Han, Y.; Pinnau, I. *J. Mater. Chem. A* **2018,** 6, (1), 30-35.
52. Chung, T. S.; Shao, L.; Tin, P. S. *Macromol. Rapid Commun.* **2006,** 27, (13), 998-1003.
53. Shao, L.; Lau, C. H.; Chung, T. *Int. J. Hydrog. Energy* **2009,** 34, (20), 8716-8722.
54. Rabbani, M. G.; El-Kaderi, H. M. *Chem. Mater.* **2012,** 24, (8), 1511-1517.
55. Shan, M.; Liu, X.; Wang, X.; Yarulina, I.; Seoane, B.; Kapteijn, F.; Gascon, J. *Sci. Adv.* **2018,** 4, (9), eaau1698.
56. Kim, D.; Tzeng, P.; Barnett, K. J.; Yang, Y. H.; Wilhite, B. A.; Grunlan, J. C. *Adv. Mater.* **2014,** 26, (5), 746-751.
57. Jorgensen, B. S.; Young, J. S.; Espinoza, B. F. *U.S. Patent 6946015B2* **2005**.
58. Young, J. S.; Long, G. S.; Espinoza, B. F. *U.S. Patent US6997971B1* **2006**.
59. Naderi, A.; Tashvigh, A. A.; Chung, T. S. *J. Membr. Sci.* **2019,** 572, 343-349.
60. Shao, L.; Chung, T.; Goh, S.; Pramoda, K. *J. Membr. Sci.* **2005,** 256, (1-2), 46-56.
61. Xiao, Y.; Shao, L.; Chung, T.; Schiraldi, D. A. *Ind. Eng. Chem. Res.* **2005,** 44, (9), 3059-3067.
62. Low, B.; Xiao, Y.; Chung, T.; Liu, Y. *Macromolecules* **2008,** 41, (4), 1297-1309.
63. Chua, M.; Xiao, Y.; Chung, T. *Sep. Purif. Technol.* **2014,** 133, 120-128.
64. Wang, H.; Chung, T.; Paul, D. R. *J. Membr. Sci.* **2014,** 458, (Supplement C), 27-35.
65. Choi, S. H.; Jansen, J. C.; Tasselli, F.; Barbieri, G.; Drioli, E. *Sep. Purif. Technol.* **2010,** 76, (2), 132-139.
66. Wang, H.; Paul, D. R.; Chung, T. *J. Membr. Sci.* **2013,** 430, 223-233.
67. Japip, S.; Liao, K. S.; Chung, T. S. *Adv. Mater.* **2017,** 29, (4), 1603833.
68. Low, B.; Xiao, Y.; Chung, T. *Polymer* **2009,** 50, (14), 3250-3258.
69. Lau, C. H.; Low, B.; Shao, L.; Chung, T. *Int. J. Hydrog. Energy* **2010,** 35, (17), 8970-8982.
70. Powell, C. E.; Duthie, X. J.; Kentish, S. E.; Qiao, G. G.; Stevens, G. W. *J. Membr. Sci.* **2007,** 291, (1-2), 199-209.
71. Shao, L.; Chung, T.; Goh, S. H.; Pramoda, K. P. *J. Membr. Sci.* **2005,** 267, (1-2), 78-89.
72. Omidvar, M.; Stafford, C. M.; Lin, H. *J. Membr. Sci.* **2019,** 575, 118-125.
73. Panapitiya, N. P.; Wijenayake, S. N.; Nguyen, D. D.; Huang, Y.; Musselman, I. H.; Balkus, K. J.; Ferraris, J. P. *ACS Appl. Mater. Interfaces* **2015,** 7, (33), 18618-18627.
74. Moon, J. D.; Bridge, A. T.; D'Ambra, C.; Freeman, B. D.; Paul, D. R. *J. Membr. Sci.* **2019,** 582, 182-193.
75. Klaehn, J. R.; Orme, C. J.; Peterson, E. S. *J. Membr. Sci.* **2016,** 515, 1-6.
76. Sanchez-Lainez, J.; Zornoza, B.; Carta, M.; Malpass-Evans, R.; McKeown, N. B.; Tellez, C.; Coronas, J. *Ind. Eng. Chem. Res.* **2018,** 57, (49), 16909-16916.
77. Naderi, A.; Tashvigh, A. A.; Chung, T. S.; Weber, M.; Maletzko, C. *J. Membr. Sci.* **2018,** 563, 726-733.
78. Hosseini, S. S.; Peng, N.; Chung, T. S. *J. Membr. Sci.* **2010,** 349, (1-2), 156-166.
79. Naderi, A.; Chung, T. S.; Weber, M.; Maletzko, C. *J. Membr. Sci.* **2019,** 591, 117292.
80. Hosseini, S. S.; Teoh, M. M.; Chung, T. S. *Polymer* **2008,** 49, (6), 1594-1603.
81. Joseph, R. M.; Merrick, M. M.; Liu, R.; Fraser, A. C.; Moon, J. D.; Choudhury, S. R.; Lesko, J.; Freeman, B. D.; Riffle, J. S. *J. Membr. Sci.* **2018,** 564,

587-597.
82. Giel, V.; Moravkova, Z.; Peter, J.; Trchova, M. *J. Membr. Sci.* **2017,** 537, 315-322.
83. Park, H. B.; Jung, C. H.; Lee, Y. M.; Hill, A. J.; Pas, S. J.; Mudie, S. T.; Van Wagner, E.; Freeman, B. D.; Cookson, D. J. *Science* **2007,** 318, (5848), 254-258.
84. Do, Y. S.; Seong, J. G.; Kim, S.; Lee, J. G.; Lee, Y. M. *J. Membr. Sci.* **2013,** 446, 294-302.
85. Zhang, C.; Koros, W. J. *Adv. Mater.* **2017,** 29, (33), 170163.
86. Omidvar, M.; Nguyen, H.; Huang, L.; Doherty, C. M.; Hill, A. J.; Stafford, C. M.; Feng, X. S.; Swihart, M. T.; Lin, H. *ACS Appl. Mater. Interfaces* **2019,** 11, (50), 47365-47372.
87. Chu, Y. H.; Yancey, D.; Xu, L. R.; Martinez, M.; Brayden, M.; Koros, W. *J. Membr. Sci.* **2018,** 548, 609-620.
88. Hosseini, S. S.; Chung, T. S. *J. Membr. Sci.* **2009,** 328, (1-2), 174-185.
89. Favvas, E. P.; Kouvelos, E. P.; Romanos, G. E.; Pilatos, G. I.; Mitropoulos, A. C.; Kanellopoulos, N. K. *J. Porous Mater.* **2008,** 15, (6), 625-633.
90. Campo, M. C.; Magalhaes, F. D.; Mendes, A. *J. Membr. Sci.* **2010,** 350, (1-2), 180-188.
91. Hatori, H.; Takagi, H.; Yamada, Y. *Carbon* **2004,** 42, (5-6), 1169-1173.
92. Cheng, Y. D.; Ying, Y. P.; Japip, S.; Jiang, S. D.; Chung, T. S.; Zhang, S.; Zhao, D. *Adv. Mater.* **2018,** 30, (47), 1802401.
93. Amooghin, A. E.; Mashhadikhan, S.; Sanaeepur, H.; Moghadassi, A.; Matsuura, T.; Ramakrishna, S. *Prog. Mater. Sci.* **2019,** 102, 222-295.
94. Kang, Z.; Peng, Y.; Qian, Y.; Yuan, D.; Addicoat, M. A.; Heine, T.; Hu, Z.; Tee, L.; Guo, Z.; Zhao, D. *Chem. Mater.* **2016,** 28, (5), 1277-1285.
95. Choi, S.; Coronas, J.; Lai, Z.; Yust, D.; Onorato, F.; Tsapatsis, M. *J. Membr. Sci.* **2008,** 316, (1-2), 145-152.
96. Li, Y.; Liang, F.; Bux, H.; Yang, W.; Caro, J. *J. Membr. Sci.* **2010,** 354, (1-2), 48-54.
97. Yang, T.; Xiao, Y.; Chung, T. S. *Energy Environ. Sci* **2011,** 4, (10), 4171-4180.
98. Zhang, C.; Lively, R. P.; Zhang, K.; Johnson, J. R.; Karvan, O.; Koros, W. J. *J. Phys. Chem. Lett.* **2012,** 3, (16), 2130-2134.
99. Hu, L.; Liu, J.; Zhu, L.; Hou, X.; Huang; Lin, H.; Cheng. *Sep. Purif. Technol.* **2018,** 205, 58-65.
100. Huang, A.; Liu, Q.; Wang, N.; Caro, J. *J. Mater. Chem. A* **2014,** 2, (22), 8246-8251.
101. Yang, T.; Shi, G.; Chung, T. S. *Adv. Energy Mater.* **2012,** 2, (11), 1358-1367.
102. Yang, T.; Chung, T. S. *Int. J. Hydrog. Energy* **2013,** 38, (1), 229-239.
103. Etxeberria-Benavides, M.; Johnson, T.; Cao, S.; Zornoza, B.; Coronas, J.; Sanchez-Lainez, J.; Sabetghadam, A.; Liu, X. L.; Andres-Garcia, E.; Kapteijn, F.; Gascon, J.; David, O. *Sep. Purif. Technol.* **2020,** 237, 116347.
104. Sanchez-Lainez, J.; Zornoza, B.; Tellez, C.; Coronas, J. *J. Membr. Sci.* **2018,** 563, 427-434.
105. Yang, T.; Chung, T. S. *J. Mater. Chem. A* **2013,** 1, (19), 6081-6090.
106. Hu, Z.; Kang, Z.; Qian, Y.; Peng, Y.; Wang, X.; Chi, C. L.; Zhao, D. *Ind. Eng. Chem. Res.* **2016,** 55, (29), 7933-7940.
107. Huang, A.; Dou, W.; Caro, J. r. *J. Am. Chem. Soc.* **2010,** 132, (44), 15562-15564.
108. Friebe, S.; Geppert, B.; Steinbach, F.; Caro, J. r. *ACS Appl. Mater. Interfaces* **2017,** 9, (14), 12878-12885.
109. Banerjee, R.; Phan, A.; Wang, B.; Knobler, C.; Furukawa, H.; O'Keeffe, M.; Yaghi, O. M. *Science* **2008,** 319, (5865), 939-943.
110. Japip, S.; Liao, K. S.; Xiao, Y.; Chung, T. S. *J. Membr. Sci.* **2016,** 497, 248-258.
111. Wijenayake, S. N.; Panapitiya, N. P.; Nguyen, C.

N.; Huang, Y.; Balkus, K. J.; Musselman, I. H.; Ferraris, J. P. *Sep. Purif. Technol.* **2014,** 135, 190-198.
112. Wijenayake, S. N.; Panapitiya, N. P.; Versteeg, S. H.; Nguyen, C. N.; Goel, S.; Balkus, K. J.; Musselman, I. H.; Ferraris, J. P. *Ind. Eng. Chem. Res.* **2013,** 52, (21), 6991-7001.
113. Diestel, L.; Wang, N. Y.; Schulz, A.; Steinbach, F.; Caro, J. *Ind. Eng. Chem. Res.* **2015,** 54, (3), 1103-1112.
114. Yang, G.; Guo, H.; Kang, Z.; Zhao, L.; Feng, S.; Jiao, F.; Mintova, S. *ChemSusChem* **2019,** 12, (19), 4529-4537.
115. Cao, L.; Tao, K.; Huang, A.; Kong, C.; Chen, L. *ChemComm.* **2013,** 49, (76), 8513-8515.
116. Sánchez‐Laínez, J.; Paseta, L.; Navarro, M.; Zornoza, B.; Téllez, C.; Coronas, J. *Adv. Mater. Interfaces* **2018,** 5, (19), 1800647.
117. Kishore, S.; Nelson, J. A.; Adair, J. H.; Eklund, P. C. *J. Alloys Compd.* **2005,** 389, (1-2), 234-242.
118. Suhaimi, H. S. M.; Leo, C. P.; Ahmad, A. L. *Chem. Eng. Technol.* **2017,** 40, (4), 631-638.
119. Villalobos, L. F.; Hilke, R.; Akhtar, F. H.; Peinemann, K. V. *Adv. Energy Mater.* **2018,** 8, (3), 1701567.